Proceedings of the ASME 2011 Conference on Smart Materials, Adaptive Structures and Intelligent Systems
SMASIS 2011
September 18-21, 2011, Scottsdale, Arizona, USA

SMASIS2011-5188

MASSIVELY PARALLEL SIMULATIONS OF CHAIN FORMATION AND RESTRUCTURING DYNAMICS IN A MAGNETORHEOLOGICAL FLUID

Steve G. Sherman Derek A. Paley Norman M. Wereley
Department of Aerospace Engineering
University of Maryland
College Park, Maryland, 20742

ABSTRACT

Magnetorheological fluids consist of micron sized iron particles mixed in a carrier fluid, and are commonly used in adaptive dampers. Current simulations of MR fluids have been limited to thousands of particle and have been unable to simulate a a practical fluid volume ($\sim$ mm^3) with a high solids loading ($\sim$ 25 vol %). In this paper, we use NVIDIA's CUDA programming environment to simulate over one million particles. Using these simulations, we can dynamically simulate chain formation and restructuring in a practical millimeter scale fluid volume with realistic solids loading. The chain structures can be characterized in terms of extent and number, as well as obtaining physical metrics such as yield stress.

Nomenclature

χ	Magnetic susceptibility
Δt	Integration time step
$\dot{\gamma}$	Shear rate
η	Fluid viscosity
$\hat{\mathbf{r}}$	Position unit vector
$\mathbf{a}_i$	Acceleration of particle i
$\mathbf{e}_x$	Unit vector in x direction
$\mathbf{F}^c_{ij}$	Contact forces between particles i and j
$\mathbf{F}^h_i$	Hydrodynamic force on particle i
$\mathbf{F}^m_{ij}$	Magnetic forces between particles i and j
$\mathbf{H}_0$	External applied field
$\mathbf{M}$	Magnetization
$\mathbf{m}$	Magnetic moment
$\mathbf{r}$	Position vector
$\mathbf{v}_\infty$	Fluid velocity
$\mathbf{v}_i$	Velocity of particle i
μ	Magnetic permeability
ϕ	Volume fraction
τ	Shear stress
τ_y	Yield stress
a	Particle radius
c	Connectivity
c/c_0	Non-dimensional connectivity
c_0	Characteristic connectivity value
C_d	Coefficient of drag
C_p	Coefficient of polarization
h	Height of volume element
k	Repulsion constant
L	Mean chain length
L/L_0	Non-dimensional chain length
L_0	Characteristic chain length
m_i	Mass of particle i
N	Number of particles
n	Spring power
Q_{ij}	Repulsion strength
r	Magnitude of position vector
R_c	Cutoff radius
Re	Reynolds Number

INTRODUCTION

Magnetorheological (MR) fluids and electrorheological (ER) fluids are non-Newtonian fluids consisting of polarized particles suspended in a carrier fluid, such as silicone, hydrocarbon based oils, glycol or hydraulic oils. In the case of MR fluids each 3-10 micron diameter ferromagnetic particle has an associated dipole. Upon application of the field, the dipoles align and interparticle forces cause chains to form. Those chains alter the fluid by increasing the viscosity. The shear stress thus becomes field dependent. A key characteristic of the shear stress vs. shear rate or flow curve, is the yield stress. The yield stress is field dependent and defined as the shear stress intercept of the high strain rate asymptote. MR fluids have found applications in dampers, clutches and any other area where a controllable fluid is desired [1–3].

Simulations are a common method of understanding the chain dynamics and how the particle structure changes. Klingenberg has a series of papers on ER fluids [4–6] that covers the basics of many of the interactions in an MR fluid. Ly et. al. present an advanced method for computing the magnetic moment, including multipole effects [7]. Spinks uses simulations to examine chain structure under a variety of fluid flow profiles [8]. Han, Feng and Owen do simulations on the particle dynamics as well as examining the fluid dynamics of the carrier fluid [9]. Mohebi and Jamasbi investigate how particle chains aggregate to form thick columnar structures [10]. Ido examines the effects of non-magnetic particles and spherocylindrical particles [11].

However, these simulations have not been extended to a full MR damper, which has the active fluid in a representative annular channel that is 10mm long, 1mm wide with a radius of 25mm. Representing a full damper would allow for the analysis of the fluid entrance and exit flows, as well as capturing the transient forces and microstructure changes. Considering the rotational symmetry, a representative fluid volume would be $10\text{mm} \times 1\text{mm} \times 1\text{mm}$. With particles of radius $a = 3.5\mu m$ at a volume fraction of $\phi = 0.35$, a simulation would require approximately 2×10^7 particles.

Existing simulations, using approximately 5000 particles, are too small scale to represent a fluid volume of that size. There are also few good numerical methods for analyzing chain formation at this scale. The standard method for examining the chain formation is looking at particle position time histories are used to show how the chains have formed, as well as the mean length of the chains. While snapshots of particle locations are useful for smaller numbers of particles, they do not scale well to domains having a million particles or more. Similarly, quantities such as mean chain length are dependent on the geometry of the simulation volume, so the values are not scale independent.

This paper aims to show the feasibility of simulations at length scales approaching a millimeter and with over one million particles. To achieve this goal, we ran our simulation code on a commercial graphics card, using NVIDIA's general purpose graphics processing unit programming (GPGPU) environment, CUDA. NVIDIA claims speedups of up to two orders of magnitude over traditional single processor code [12], and we use that ability to run two orders of magnitude more particles than existing simulations [5, 7–11]. To analyze the particle chain formation, we measure the chain length and connectivity, and nondimensionalize the results by comparing it to an ideal case.

MAGNETORHEOLOGY

MR fluids are magnetic particles suspended in a carrier fluid. Particles are typically made out of iron, cobalt, nickel or an alloy of these. Particle concentration is measured using volume fraction, ϕ, which is the ratio of particle volume to bulk volume. Under the application of an external magnetic field, $\mathbf{H}_0$, particle chains form in the fluid and the fluid thickens. One of the standard descriptions of an MR fluid is as a Bingham plastic, described by

$$\tau = \tau_y + \eta\dot{\gamma} \qquad \dot{\gamma} \geq 0, \tag{1}$$

where τ is stress, τ_y is yield stress, and $\dot{\gamma}$ is shear rate.

A typical MR device has the fluid flowing through a small millimeter scale gap. There are two typical flow profiles for flow through this gap, a shear mode (Couette flow) and a flow mode, (Pouisieulle flow). In shear mode, which is studied here, the upper surface of the gap is moving, causing a linear flow profile. Assuming a no slip condition at the walls,

$$\mathbf{v}_\infty = \dot{\gamma}\, y\, \mathbf{e}_x, \tag{2}$$

where y is the distance from the stationary wall, and $\mathbf{e}_x$ is a unit vector pointing in the x direction.

MR fluids are typically simulated as paramagnetic spherical particles suspended in a non-magnetic viscous fluid under an external magnetic field. The magnetic field induces a magnetic moment in the particles, whose interactions cause chains to form in the fluid. Typically the induced moment is modeled as a dipole, but Ly [7] employs the fast multipole method to compute higher order effects.

A qualitative diagram of chain formation is presented in Fig. 1. In the absence of field, the particles are suspended in the fluid at random. Upon application of field, the particles form chains from top to bottom. These chains are the mechanism by which force is applied to the upper plate. Under shear, the particle chains whose ends are pinned to the upper and lower surfaces become strained, and eventually break. As the broken portion travels, it will eventually reconnect to form a new chain.

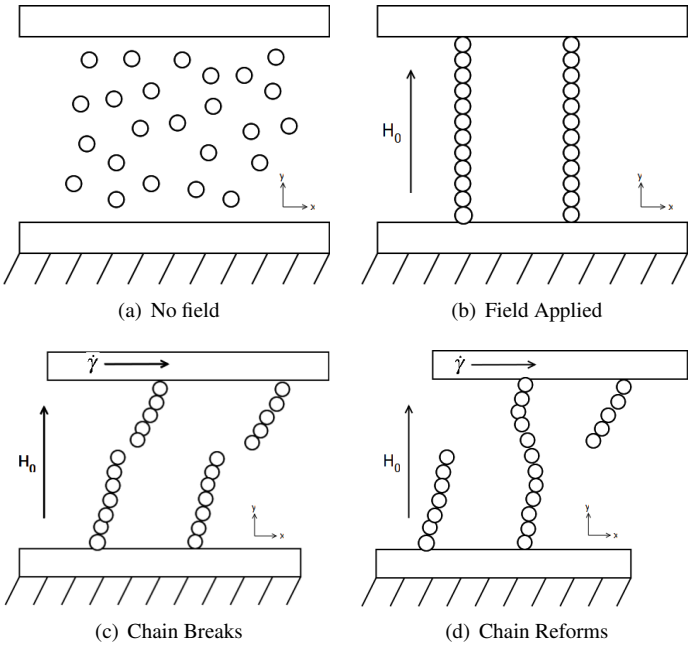

(a) No field (b) Field Applied

(c) Chain Breaks (d) Chain Reforms

FIGURE 1. CHAIN FORMATION

SIMULATION MODEL

Magnetorheological fluids can be modeled using finite element analysis, or a discrete element approach, where the equations of motion of the iron particles are integrated. The discrete element method allows investigation of the chain forming dynamics of the particle, which helps give insight into the mechanics of the fluid.

The primary forces affecting the particles are magnetic, collision and hydrodynamic forces. Other factors, such as buoyancy force and Brownian motion can be neglected, without loss of generality, according to Klingenberg [4]. Climent and Maxey present a model with Brownian motion as well as fluid disturbances caused by particle movement [13].

Fluid Volume

The simulations in this study use a cubic simulation volume. The external field $\mathbf{H}_0$ points in the positive y direction. The upper surface shears in the positive x direction, in the direction of fluid flow. Particles touching the upper and lower surfaces are pinned. All other surfaces have periodic boundary conditions. Figure 2 shows the layout of the simulation volume used in this study with fluid flowing according to (2). Shear stress, τ, is the sum of all forces in the x direction on the upper layer of pinned particles divided by the area of the upper surface.

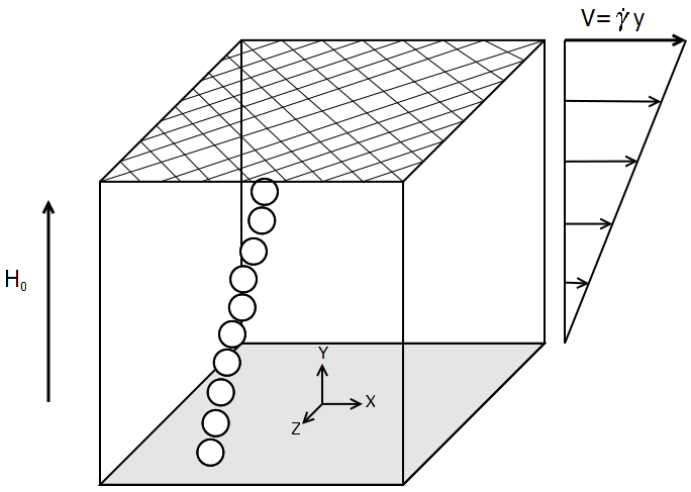

FIGURE 2. SIMULATION VOLUME

Magnetic Forces

Starting from Maxwell's equations for magnetic fields, and observing that there are no currents or charges, we can write Maxwell's equations: $\nabla \times \mathbf{H} = 0$ and $\nabla \cdot \mathbf{B} = 0$. If we assume that the permeability of the medium, μ, is linearly isotropic, $\mathbf{H}$ and $\mathbf{B}$ are related by

$$\mathbf{B} = \mu \mathbf{H}. \tag{3}$$

If a point dipole i is inserted in the field with magnetic moment $\mathbf{m}_i$, at point $\mathbf{r}_i$ relative to the dipole, the emitted field is

$$\mathbf{H}_i = \frac{1}{4\pi} \frac{3(\mathbf{m}_i \cdot \hat{\mathbf{r}}_i)\hat{\mathbf{r}}_i - \mathbf{m}_i}{r_i^3}, \tag{4}$$

where $r_i = ||\mathbf{r}_i||$. The force on a point dipole, $\mathbf{m}_j$, from point dipole, $\mathbf{m}_i$, can be computed from

$$\mathbf{F}_{ij}^m = \nabla(\mathbf{m}_j \cdot \mathbf{B}_i). \tag{5}$$

Let $\mathbf{r}_{ij}$ be the position of particle i relative to particle j. Using (4) and (5), we get,

$$\begin{aligned} \mathbf{F}_{ij} = \frac{3\mu_f}{4\pi r_{ij}^4}[&(\mathbf{m}_i \cdot \hat{\mathbf{r}}_{ij})\mathbf{m}_j + (\mathbf{m}_j \cdot \hat{\mathbf{r}}_{ij})\mathbf{m}_i \\ &+ (\mathbf{m}_i \cdot \mathbf{m}_j)\hat{\mathbf{r}}_{ij} - 5(\mathbf{m}_i \cdot \hat{\mathbf{r}}_{ij})(\mathbf{m}_j \cdot \hat{\mathbf{r}}_{ij})\hat{\mathbf{r}}_{ij}]. \end{aligned} \tag{6}$$

Each dipole also produces a torque on the other. The torque on $\mathbf{m}_j$ from $\mathbf{m}_i$ is

$$\mathbf{T}_{ij} = \mathbf{m}_j \times \mathbf{B}_i. \tag{7}$$

Since we assume that the particles in the fluid are paramagnetic beads which have no intrinsic magnetic moment, the magnetic moment is always aligned with the field and there is no torque. As a result, the rotational dynamics of the particles are ignored.

Magnetic Moments

Magnetic susceptibility is the ratio of permeabilities of a material. There also exists an effective susceptibility, χ_{eff}, which is the amount the particle will actually be magnetized:

$$\chi = \frac{\mu_{\text{particle}}}{\mu_{\text{fluid}}}, \text{ and } \chi_{\text{eff}} = \frac{3(\chi-1)}{\chi+2}. \tag{8}$$

For a linearly susceptible material in a magnetic field, the magnetization, $\mathbf{M}$ is related to the $\mathbf{H}$ field through susceptibility, χ, according to

$$\mathbf{M} = \chi \mathbf{H}. \tag{9}$$

Assuming a constant external field, integrating over the volume of the particle yields the magnetic moment, $\mathbf{m}$.

$$\mathbf{m} = \frac{4}{3}\pi a^3 \chi_{\text{eff}} \mathbf{H} = C_p \mathbf{H} \tag{10}$$

Unfortunately, the presence of other dipoles in the MR fluid means that the field is not constant throughout the particle. Exact solutions are possible, revealing extensive multipole effects [14]. These are extremely expensive to compute, and are impractical for the high particle count simulations we are doing. Two common approximations for the exact solution are the fixed dipole method and the mutual dipole method.

In the fixed dipole model, where the field from other particles is not considered, we have

$$\mathbf{m}_i = C_p \mathbf{H}_0. \tag{11}$$

Since the strong external field contributes most of the energy of the magnetic moment, it is fairly accurate for particles far away from each other, but at distances less than a diameter it becomes inaccurate.

A more accurate version is the mutual dipole model. In the mutual model, the magnetic moment calculation considers the contributions from it's neighboring particles. Here, $\mathbf{m}_i^k$ is the value of $\mathbf{m}_i$ on the kth iteration. We have,

$$\mathbf{m}_i^{k+1} = C_p \left(\mathbf{H}_0 + \sum_{j=1, j\neq i}^{n} \mathbf{H}_{ij}(\mathbf{m}_i^k, \mathbf{m}_j^k) \right). \tag{12}$$

Equation 12 converges rapidly, with a relative error of 10^{-5} within 3 iterations. Han, Feng and Owen show [9] that this model results in a 77.78% increase in peak attractive force, and a 20.99% decrease in peak repulsion force. Experimental measurements by Gast show the importance of this effect [15]. Qualitatively, the mutual dipole model leads to an increase in particle chains agglomerating to form thicker strands.

Repulsive Forces

To keep the particles separated, a repulsive force must be applied. In MR fluid simulations, two popular choices are some sort of hard spring repulsion and an exponentially decaying repulsion potential. The hard spring model can be parameterized by k, a repulsion constant, and n a power for the spring.

$$\mathbf{F}_{ij}^c = -k(1-\frac{r}{2a})^n \hat{\mathbf{r}}_{ij} \text{ if } r_{ij} < 2a \text{ and } 0 \text{ if } r_{ij} \geq 2a \tag{13}$$

Since there is no force at the particle boundary, one of the downsides of this model is that there is some degree of overlap between particles. In order to keep the level of overlap small, the spring must be extremely stiff, causing difficulties in integration.

The exponential-decay model solves both of these problems. At the particle boundary it provides the required force to keep the particles separated and since it extends outside the particle boundary, it is much softer and thus easier to integrate. The exponential decay model is

$$\mathbf{F}_{ij}^c = Q_{ij} \exp(-k(1-\frac{r}{2a}))\hat{\mathbf{r}}_{ij}. \tag{14}$$

It is described by Q_{ij}, the magnitude of the maximum attractive force, and a repulsive spring constant k. The value of Q_{ij} can be computed from (6), and yields

$$Q_{ij} = \frac{3\mathbf{m}_i \cdot \mathbf{m}_j \mu_f}{8a^4}. \tag{15}$$

A flaw of the exponential decay model is that it emits a force outside the particle, and so moves the bottom of the repulsion potential away from the surface of the particle. While this distance is not large, it can have substantial effects. Small scale numerical experiments showed that for values of $k = 12$, this separation inhibited chain agglomeration, making it more likely that more the particle chains to be thin monofilaments. The observed effects on fluid stress were small. For the large scale CUDA simulations described below, we use the exponential decay model with $k = 20$.

TABLE 1. SIMULATION PARAMETERS

N	h (mm)	Processing Time (s)
1000000	0.896	1.69s
103100	0.420	0.179s
10480	0.196	0.025s
1380	0.098	0.011s

Hydrodynamic Forces and Equations of Motion

The hydrodynamic force used here is Stokes Drag, because we are dealing with an extremely small particle in a fluid with an extremely low Reynolds number (10^{-2}) . This is a common choice for these simulations [4–6, 9]. We have

$$\mathbf{F}_i^h = -6\pi a\eta(\mathbf{v}_i - \mathbf{v}_\infty) = -C_d(\mathbf{v}_i - \mathbf{v}_\infty). \tag{16}$$

The equations of motion for a particle in an MR fluid are

$$m_i\mathbf{a}_i = \mathbf{F}_i^h + \sum_{j=1, j\neq i}^{n} \left(\mathbf{F}_{ij}^c + \mathbf{F}_{ij}^m\right) \tag{17}$$

Since the mass of the particle is extremely low, on the order 10^{-10} g, and the force on the particle is on the scale of 10^{-6} N, the left-hand side of (17) is extremely small. A similar analysis can be done on the Reynolds number, *Re*, which is around 10^{-2}, showing that viscous forces dominate inertial forces. Setting the left hand side equal to zero, we now have a balance of forces that needs to be solved. Observing that magnetic forces and contact forces are solely functions of relative particle position, and we can solve for velocity using (16) and (17).

$$\mathbf{v}_i = \mathbf{v}_\infty + \frac{1}{C_d}\sum_{j=1, j\neq i}^{n} \left(\mathbf{F}_{ij}^c + \mathbf{F}_{ij}^m\right) \tag{18}$$

We use this simplified equation to integrate particle trajectories using the trapezoidal method. The trapezoidal method is a second order solver, and its simplicity make it ideal for computation on the GPU.

SIMULATION RESULTS

Simulations were run on a NVIDIA GTX 480. All steps in the integration process were performed on the GPU using single precision floating point values. Particle initial conditions are set randomly and then initial overlaps are resolved using a linear spring model. All simulations were done with $\mu_f = \mu_0 = 4\pi 10^{-7}$ H/m and $\mu_p = 2.513 \times 10^{-3}$ H/m giving a value of $\chi = 2000$. The applied external field, $\mathbf{H}_0$, had a magnitude of 100 kA/m. The fluid viscosity was $\eta = 0.25$ Pa s. The time step for all simulations was $\Delta t = 5 \times 10^{-8} s$. The particle radius was $a = 3.5\mu$m for all simulations. A repulsion constant of $k = 20$ was used for the exponential force model.

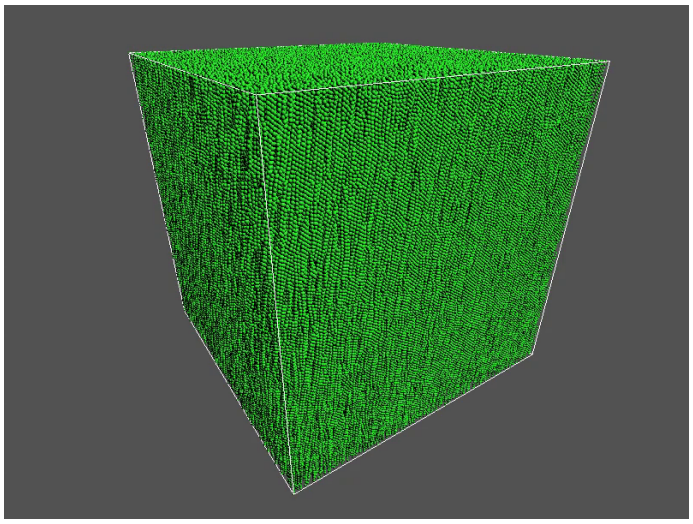

FIGURE 3. ONE MILLION PARTICLES

Observe that the longest range interaction is the induced magnetic moment, which scales with r^{-3}. So considering an infinite one dimensional particle chain, the force scales with the sum

$$\mathbf{H} \cong \frac{\mathbf{m}}{2\pi}\left(\frac{1}{(2a)^3} + \frac{1}{(4a)^3} + \frac{1}{(6a)^3} + \frac{1}{(8a)^3)} + ...\right) \tag{19}$$

Truncating the sum in (19) after four terms yields a value with relative error of 2.02%. Consequently, a cut off radius for particle interactions, R_c, was set to $8a$. We use three iterations of the mutual dipole model to solve for the magnetic moment. All simulations were conducted at a volume fraction of $\phi = 0.250$ (25 vol%) across four orders of magnitude, allowing us to compare runs from $N = 10^3$ to $N = 10^6$. Table 1 presents the size of the cubic simulation volumes and the execution time per timestep on a GTX 480 for each order of magnitude. Figure 3 is a screenshot of the program graphical output.

Non-dimensional Chain Metrics

Measuring the chain structure is extremely difficult for large particle counts. As Fig. 3 shows, it is quite difficult to distinguish which particles are connected to what, and the finer details of the chain structure. Metrics such as chain length and connectivity are highly dependent on the geometry of the volume [7]. Other metrics, such as the Christiansen uniformity coefficient,

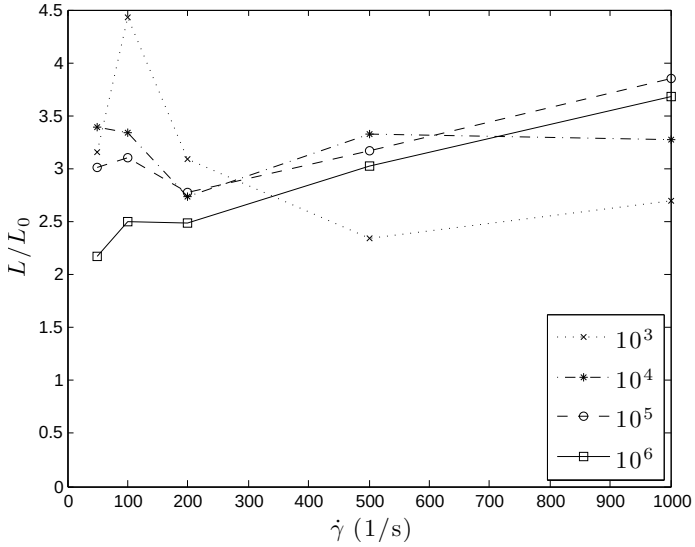

FIGURE 4. CHAIN LENGTH VS. SHEAR RATE AT $\phi = 0.25$

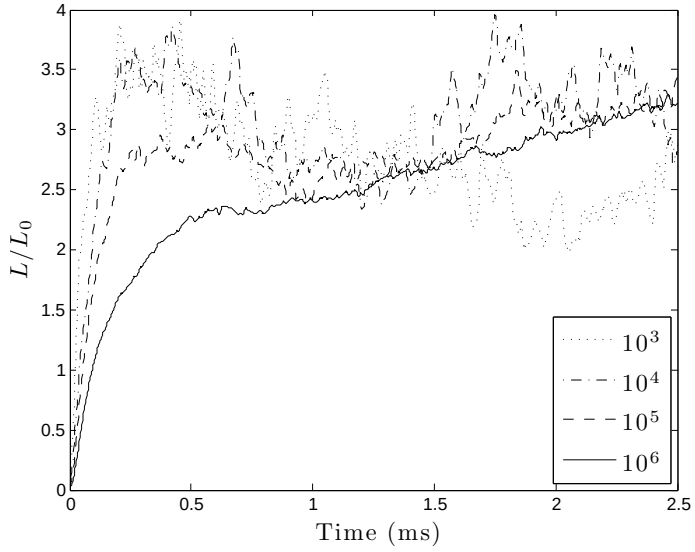

FIGURE 5. CHAIN LENGTH VS. TIME AT $\phi = 0.25$

have proven ineffective [11]. We consider particles i and j to be connected if $r_{ij} < 2.2a$. Connectivity, c, is the total number of connections, and mean chain length, L, is the mean size of the graphs formed by particle connections.

If we consider a simulation volume spanned by single width monofilament chains spanning top to bottom, we can compute characteristic values of connectivity and chain length. We have

$$c_0 = N\left(1 - \frac{2a}{h}\right), \tag{20}$$

and

$$L_0 = \frac{h}{2a}. \tag{21}$$

These values allow us to compute a non-dimensional value of connectivity, c/c_0 and a non-dimensional chain length L/L_0. Non-dimensional connectivity is an improvement over mean connectivity as it reduces the effect of simulation volume height limiting the length of chains. Similarly, non-dimensional chain length is an improvement over the raw value as it allows comparison of chain lengths in different height simulation volumes.

Figure 4 plots the steady state non-dimensional chain length versus shear rate for different particle counts. If there were only monofilament chains we would expect a value of $L/L_0 = 1$. There is an approximate steady state value of $L/L_0 = 3.5$, indicating that each chain has the length equivalent to three monofilament chains. This high value is a strong indicator of chain agglomeration into thick columnar structures.

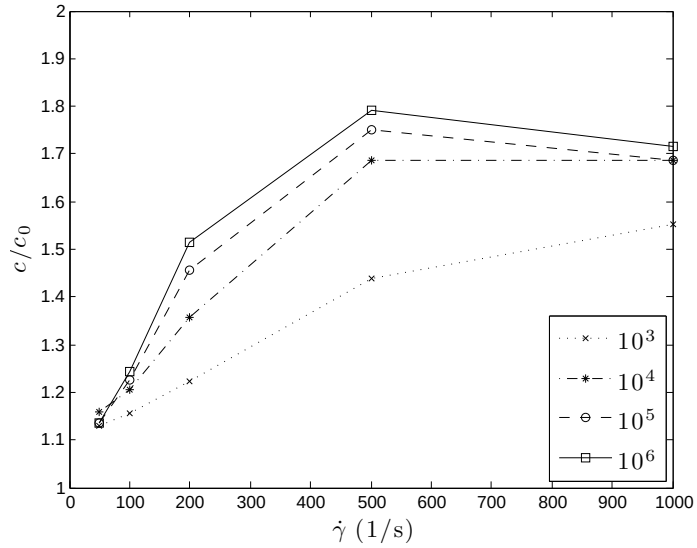

FIGURE 6. CONNECTIVITY VS. SHEAR RATE AT $\phi = 0.25$

Figure 5 is a time history of non-dimensional chain length at a shear rate $\dot{\gamma} = 200\text{s}^{-1}$. It shows how an increase in N at a constant volume fraction gives smoother data while having similar non-dimensional values.

Figure 6 plots steady state non-dimensional connectivity versus shear rate across simulation scales. Under the monofilament assumption, we would expect of a value of $c/c_0 = 1$. At low shear rates, we observe a value of $c/c_0 = 1.15$ indicating that initially the number of adjacent particles is consistent with the monofilament model. However, connectivity increases at high shear rates, reaching 1.7, indicating that more particles are in

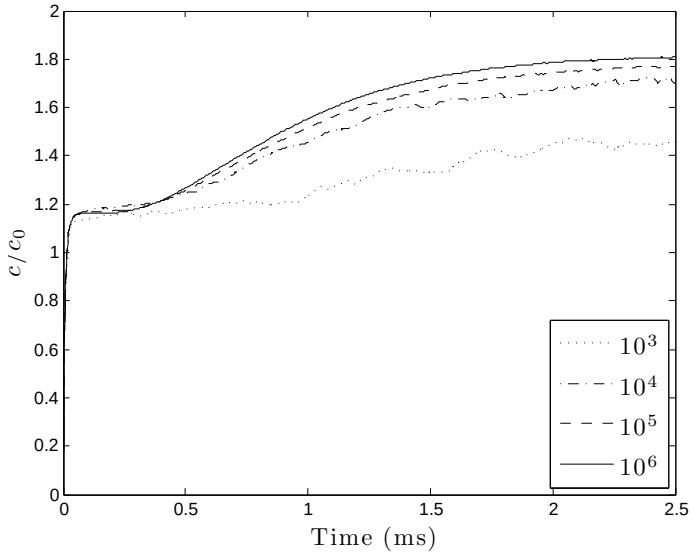

FIGURE 7. CONNECTIVITY VS. TIME AT $\phi = 0.25$

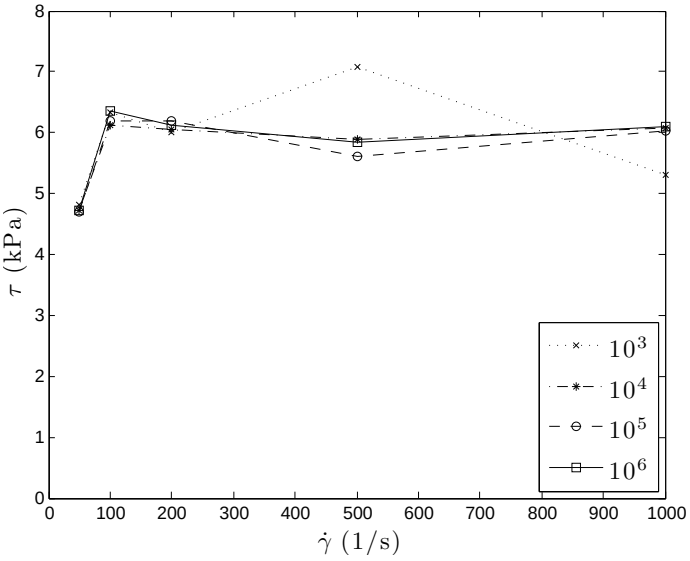

FIGURE 8. STRESS VS. SHEAR RATE AT $\phi = 0.25$

contact as the fluid is sheared, and thus in a thicker columnar structure. The rise in connectivity with N could be explained by the mechanism reported in [10], where increases in simulation volume height helped single strand chains zipper together to form thick columnar structures.

Figure 7 plots the time response of non-dimensional connectivity at a shear rate of $\dot{\gamma} = 500\text{s}^{-1}$. There is an initial plateau at $t = 0.2ms$ of $c/c_0 = 1.2$ followed by slow rise in value as the chains are sheared, approaching a value of $c/c_0 = 1.8$. This indicates that thin chains form initially and then come into contact with many more particles as they are sheared.

Figure 8 plots peak stress versus shear rate across the same simulation scales as Fig. 4 and 6. Expected yield stress for a fluid of our parameters would be in the 5 kPa range [16], so the simulated result of 6 kPa is consistent with these results. This is consistent with experimental evidence that at low field strengths dipole models are sufficient [15, 17, 18]. The shape of the shear stress vs. strain rate (flow) curve is similar to those measured experimentally [19].

Figure 9 plots stress versus time at a shear rate of $\dot{\gamma} = 500\text{s}^{-1}$, illustrating how higher particle counts result in smoother time histories. In low particle count simulations, the consequences of a chain breaking are more significant because the number of chains is smaller.

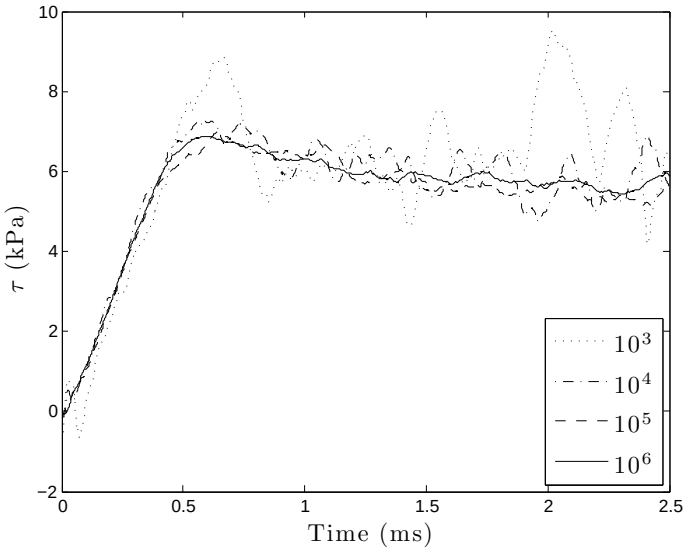

FIGURE 9. STRESS VS. TIME AT $\phi = 0.25$

CONCLUSION

This paper demonstrates the feasibility of simulating one million particles with NVIDIA's CUDA programming environment. We were able to compute properties such as yield stress, chain number and edge number using simulation results. These non-dimensional parameters for measuring the chain formation of the fluid were created to gain insight into the microstructure of the fluid across simulation scales.

1. Stress calculations show that our present method generates stresses of 6 kPa which are consistent with the values of 5 kPa we would expect from [16].

2. The non-dimensional connectivity and non-dimensional chain length are effective metrics of chain formation and are independent of simulation scale. These values indicate that thick columnar structures are forming in the fluid. We used these metrics to determine that the response time for chain formation at an

external field strength of 100 kA/m was nominally 0.2 ms.

Future work includes examining the response of stress, chain number and edge number to fluid parameter such as external field strength, and particle size, as well as sensitivity of the simulation results to modeled physics.

REFERENCES

[1] Pang, L., Kamath, G., and Wereley, N., 2001. "Analysis and testing of a linear stroke magnetorheological damper". *AIAA Journal,* ***39***(7), pp. 1240–1253.

[2] Carlson, J. D., Catanzarite, D., and Clair, K. A. S., 1996. "Commercial Magnetorheological Fluid Devices". *International Journal of Modern Physics B,* ***10***(23-24), pp. 2857–2865.

[3] Choi, Y.-T., and Wereley, N. M., 2003. "Vibration control of a landing gear system featuring electrorheological/magnetorheological fluids". *Journal of Aircraft,* ***40***(3), May, pp. 432–439.

[4] Klingenberg, D. J., van Swol, F., and Zukoski, C. F., 1989. "Dynamic simulation of electrorheological suspensions". *The Journal of Chemical Physics,* ***91***(12), pp. 7888–7895.

[5] Klingenberg, D. J., van Swol, F., and Zukoski, C. F., 1991. "The small shear rate response of electrorheological suspensions. I. Simulation in the point dipole limit". *The Journal of Chemical Physics,* ***94***(9), pp. 6160–6169.

[6] Klingenberg, D. J., van Swol, F., and Zukoski, C. F., 1991. "The small shear rate response of electrorheological suspensions. II. Extension beyond the point dipole limit". *The Journal of Chemical Physics,* ***94***(9), pp. 6170–6178.

[7] Ly, H., 1999. "Simulations of particle dynamics in magnetorheological fluids". *Journal of Computational Physics,* ***155***(1), Oct., pp. 160–177.

[8] Spinks, J. M., 2008. "Dynamic simulation of particles in a magnetorheological fluid". Masters, Naval Postgraduate School, May.

[9] Han, K., Feng, Y. T., and Owen, D. R. J., 2010. "Three-dimensional modelling and simulation of magnetorheological fluids". *International Journal for Numerical Methods in Engineering,* ***84***(11), Dec., pp. 1273–1302.

[10] Mohebi, M., Jamasbi, N., and Liu, J., 1996. "Simulation of the formation of nonequilibrium structures in magnetorheological fluids subject to an external magnetic field". *Physical Review E,* ***54***(5), Nov., pp. 5407–5413.

[11] Ido, Y., Inagaki, T., and Yamaguchi, T., 2010. "Numerical simulation of microstructure formation of suspended particles in magnetorheological fluids.". *Journal of physics. Condensed matter,* ***22***(32), Aug., p. 324103.

[12] Nvidia, 2011. NVIDIA CUDA C Programming Guide. Tech. rep., NVIDIA Inc.

[13] Climent, E., Maxey, M. R., and Karniadakis, G. E., 2004. "Dynamics of self-assembled chaining in magnetorheological fluids". *Langmuir,* ***20***(2), Jan., pp. 507–513.

[14] Keaveny, E., and Maxey, M., 2008. "Modeling the magnetic interactions between paramagnetic beads in magnetorheological fluids". *Journal of Computational Physics,* ***227***(22), Nov., pp. 9554–9571.

[15] Furst, E., and Gast, A., 2000. "Micromechanics of magnetorheological suspensions". *Physical Review E,* ***61***(6), June, pp. 6732–6739.

[16] Mantripragada, S., Wang, X., Gordaninejad, F., Hu, B., and Fuchs, A., 2007. "Rheological properties of novel magnetorheological fluids". *International Journal of Modern Physics B,* ***21***(28-29), p. 4849.

[17] Furst, E., and Gast, A., 1999. "Micromechanics of dipolar chains using optical tweezers". *Physical Review Letters,* ***82***(20), May, pp. 4130–4133.

[18] Furst, E., and Gast, A., 2000. "Dynamics and lateral interactions of dipolar chains". *Physical Review E,* ***62***(5), Nov., pp. 6916–6925.

[19] Genç, S., and Phulé, P. P., 2002. "Rheological properties of magnetorheological fluids". *Smart Materials and Structures,* ***11***(1), Feb., pp. 140–146.